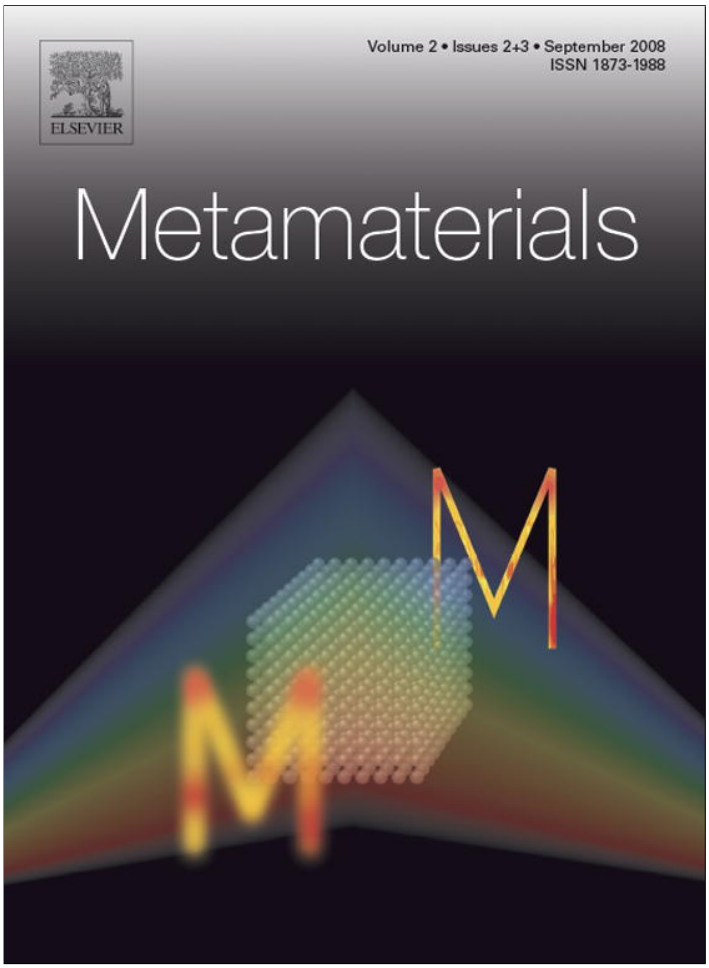

Available online at www.sciencedirect.com
ScienceDirect
Metamaterials 2 (2008) 122–134
Metamaterials
www.elsevier.com/locate/metmat

Three-frequency parametric amplification in magneto-inductive ring resonators

R.R.A. Syms *, L. Solymar, I.R. Young

Optical and Semiconductor Devices Group, EEE Department, Imperial College London, Exhibition Road, London SW7 2AZ, UK

Received 14 December 2007; received in revised form 7 March 2008; accepted 10 March 2008
Available online 16 March 2008

Abstract

Parametric amplification of magneto-inductive (MI) waves propagating in magnetically coupled chains of nonlinear *L–C* resonators is studied. Analysis is first presented for a three-frequency travelling wave scheme in which the signal, idler and pump all propagate as MI waves. The effect of de-coupling the idlers is then considered and it is shown that this configuration relaxes the standard phase matching condition. Confirmation of the theory is provided using low-frequency PCB unit cells containing varactor diodes. The cells are characterised individually and then arranged as a 16-element ring resonator. Frequency matching and selective amplification of the primary resonance is demonstrated. The primary resonance can be excited using the field of a rotating magnetic dipole, and an application in magnetic resonance imaging is described.

PACS: 41.20.Jb

Keywords: Metamaterial; Magneto-inductive wave; Parametric amplifier; Varactor

1. Introduction

Following developments by Veselago [1] and Pendry et al. [2], considerable interest has been shown in the behaviour of periodic structures known as metamaterials. Metamaterials can have novel properties such as negative values of ε and μ at electromagnetic frequencies that are achieved by virtue of their physical arrangement rather than their constituents. For example, so-called 'left-handed' metamaterials exhibit negative refraction.

One simple metamaterial is a periodic arrangement of magnetically coupled *L–C* resonators, which can support a travelling magnetic field known as a magneto-inductive (MI) wave. The theory of MI waves has been developed for one [3] or more [4,5] dimensions, and interactions with electromagnetic waves [6] and radiation effects [7] have been considered. Experimental confirmation of the major effects has been obtained using low-frequency circuits [8–12], and MI waves have been observed in other metamaterials such as 'Swiss rolls' [13]. Applications in splitters [14], filters [15,16], ring resonators [17] and lenses for sub-wavelength imaging [18,19] are emerging. Parametric amplification has been proposed to reduce propagation losses [20], inherent in electromagnetic metamaterials. MI waves have analogies with waves in arrays of cylinders [21,22] and dipoles [23] and

* Corresponding author. Tel.: +44 207 594 6203; fax: +44 207 594 6308.
E-mail address: r.syms@imperial.ac.uk (R.R.A. Syms).

1873-1988/$ – see front matter © 2008 Elsevier B.V. All rights reserved.
doi:10.1016/j.metmat.2008.03.003

other periodic structures [24], and direct correspondence with waves in arrays of open loop [25] and split ring resonators [2,26–28]. There are even analogies with chains of optical cavities [29].

Recently, tunable elements such as varactor diodes have been used to provide electrically controllable metamaterials [30–32]. Theoretical and experimental studies of parametric processes in metamaterials have also been conducted [33–37], showing that classical effects such as amplification and second harmonic generation may be obtained, together with new effects such as changes from left- to right-handed behaviour.

The propagation of waves in periodic structures is of course an old field, best exemplified by Brillouin's classic work [38], and transmission line representations are often used to describe metamaterials [39–41], exactly as they were for generations of older ladder networks. Parametric amplification is also an old field, brought to prominence by Manley and Rowe in the late 1950s [42,43] but with much earlier roots. A review from 1960 [44] contains 200 references, the first due to Faraday in 1831.

Early parametric amplifiers were lumped element circuits that transferred energy from a pump at angular frequency $\omega_P = 2\omega_S$ to a signal at ω_S using two resonators coupled by a varactor diode, which was then being developed [45]. However, these so-called 'degenerate amplifiers' suffered from the serious drawback of requiring the pump to be phase locked to the signal, an unrealistic scenario [46,47]. Consequently, they were rapidly discarded in favour of three-frequency amplifiers, which avoided any requirement for phase locking using a two-step energy conversion via an additional idler resonator operating at ω_I [48]. Frequencies were then raised, by replacing lumped elements with resonant cavities [49,50], and bandwidth was increased using double-tuned circuits [51,52]. A summary of lumped-element circuits can be found in [53].

Exploration of ladder filters [54,55] led to development of lumped-element travelling wave parametric amplifiers [56–58] that are the true precursors of nonlinear metamaterials. Following a classic analysis by Tien [59], a transition was made to continuous travelling wave amplifiers based on ferromagnetic [60] and space charge [61,62] waves. Parametric methods have of course been heavily exploited in optics [63]. Developments in other fields continue with Josephson junction amplifiers [64,65], amplifiers for acoustic waves [66] and most recently microelectromechanical (MEMS) devices [67].

The use of a variable reactance promised low noise amplification, a feature that was extremely attractive for astronomy and space communications [68]. A variety of instrumentation applications have been proposed, including amplification of electron spin resonance [69] and ac magnetic [70] signals. In this paper, we consider a further detection application, based on the ability of a MI ring resonator to couple to the field of a precessing magnetic dipole [17]. Such an arrangement is strongly analogous to the 'birdcage' detector for magnetic resonance imaging (MRI) developed by Hayes et al. [71], in which the dipole field is coupled to the primary resonance of a backward wave on a ladder-structured ring resonator [72,73]. An alternative involving a forward wave has also been developed [74].

Here, our aim is to develop a scheme for parametric amplification that might improve signal-to-noise ratio in MRI. The arrangement for parametric amplification of MI waves presented in [20] involved two frequencies propagating in two concentric rings and a crude demonstration of two-frequency amplification on a ring resonator with a non-propagating pump was made recently [75]. However, for practical use a three-frequency scheme is clearly required and here we demonstrate a suitable approach.

In Section 2, we provide a brief introduction to MI waves and ring resonators, reviewing earlier work [3,4,17]. In Section 3, we also review three-frequency parametric amplification, largely following [53]. In Section 4, we propose a three-frequency travelling wave amplification scheme for MI waves, demonstrate the relation to earlier work, and develop a modification based on de-coupled idlers that is more suitable for ring resonators. In Section 5, we describe the construction of a parametrically amplified magneto-inductive ring using varactor diodes and printed circuit board inductors, and present experimental results that demonstrate selective amplification of ring modes. Conclusions are drawn in Section 6.

2. Magneto-inductive waves and ring resonators

Fig. 1a shows a one-dimensional magneto-inductive waveguide [3], which consists of a set of capacitively loaded loops with a regular separation "a". The array is infinitely long, and each element is coupled magnetically to its nearest neighbours. Fig. 1b shows the equivalent circuit. The elements are modelled as resonant circuits consisting of a capacitor C, an inductor L and a resistor R accounting for loss. Using Kirchhoff's voltage law to relate the currents I_n in neighbouring elements, the

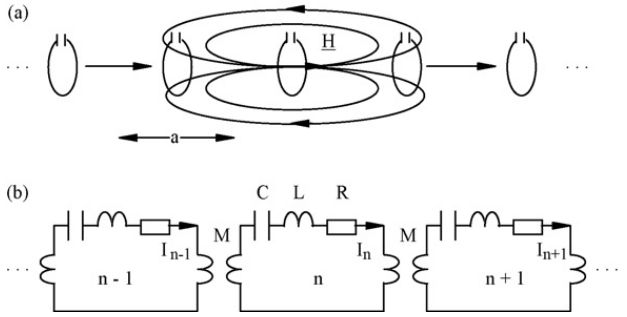

Fig. 1. (a) Magneto-inductive waveguide with nearest-neighbour coupling; (b) equivalent circuit.

dispersion equation may be obtained as:

$$\left\{1 - \frac{\omega_0^2}{\omega^2} - \frac{j}{Q}\right\} + \kappa\cos(ka) = 0 \tag{1}$$

Here ω is the angular frequency, $\omega_0 = (LC)^{-1/2}$ is the corresponding resonant frequency and $Q = \omega_0 L/R$ is the quality factor. The constant $\kappa = 2M/L$ is the coupling coefficient, where M is the mutual inductance. "κ" may be positive or negative, depending on whether the loops are arranged in the axial or the planar (edge-coupled) configuration. In the former case, a forward wave is obtained, and in the latter a backward wave. The propagation constant is $k = k' - jk''$, where $k'a$ and $k''a$ are the phase shift and attenuation per element, respectively. Eq. (1) may of course be solved exactly. However, when losses are low, we may write:

$$\left(1 - \frac{\omega_0^2}{\omega^2}\right) + \kappa\cos(k'a) \approx 0$$
$$k''a \approx \frac{1}{\kappa Q \sin(k'a)} \tag{2}$$

The result is a single propagating wave solution, which exists over the frequency band $1/(1+|\kappa|) \le (\omega/\omega_0)^2 \le 1/(1-|\kappa|)$ whose extent depends on the value of κ, and hence on the strength of the mutual inductance between the loops. Low losses require both a high Q-factor and a high coupling coefficient, and losses are maximised at the band edges and minimised at the band centre. Higher losses, which require full solution of Eq. (1), result in lossy propagation outside the band. For backward waves, $k''a$ is negative, and $|k''a|$ is a more realistic indicator of loss. Interactions between nth nearest neighbours may be modelled by introducing additional coupling terms κ_n into Eq. (1) to obtain [11].

$$\left\{1 - \frac{\omega_0^2}{\omega^2} - \frac{j}{Q}\right\} + \sum_n \kappa_n \cos(nka) = 0 \tag{3}$$

Fig. 2a shows a magneto-inductive ring resonator [17]. Here a set of N resonant elements is arranged in a polygon. The ring will clearly be resonant when the phase accumulated in a round trip is a whole number of multiples of 2π, so that $k'Na = 2\mu\pi$, where μ is an integer (the mode number). For a ring with an even number of elements, modal degeneracy implies that there will be $N/2+1$ distinct resonances, whose propagation constants k'_μ are:

$$k'_\mu a = \frac{2\mu\pi}{N} \quad (\mu = 0, 1, \ldots, N/2) \tag{4}$$

Once these values of $k'_\mu a$ are known, the corresponding angular frequencies ω_μ may be obtained from the dispersion equation. In the low loss case, Eq. (2) gives:

$$\frac{\omega_\mu}{\omega_0} = \frac{1}{\sqrt{1+\kappa\cos(k'_\mu a)}} \tag{5}$$

For example, the full line in Fig. 2b shows the dispersion characteristic of a low-loss backward MI waveguide with a coupling coefficient $\kappa = -0.3$, together with a graphical determination of the resonances of a 16-element ring. The primary resonance ($\mu = 1$) is at $k'a = \pi/8$. This resonance may be coupled to a magnetic dipole rotating at the centre of the ring at the same angular frequency. The primary effect of non-nearest-neighbour coupling is to change the dispersion

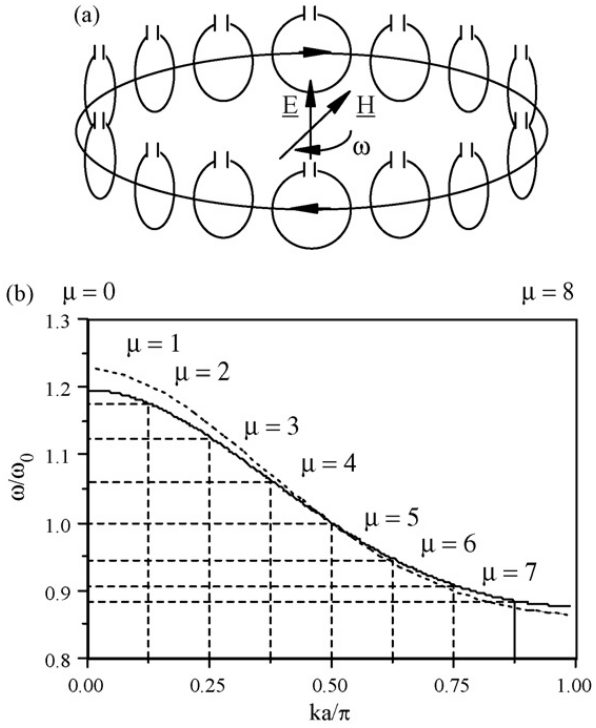

Fig. 2. (a) MI wave ring resonator; (b) MI wave dispersion characteristic, and resonances for a 16-element ring. Full line: $\kappa_1 = -0.3$, $\kappa_2/\kappa_1 = 0$. Dashed line: $\kappa_1 = -0.3$, $\kappa_2/\kappa_1 = 1/9$.

characteristic (see for example [73]), although a secondary effect is to introduce higher order modes [11]. The dashed line shows the effect of a second neighbour coupling coefficient $\kappa_2/\kappa_1 = 1/9$, which increases high-frequency propagation.

3. Three-frequency parametric amplification

Fig. 3a shows the usual arrangement for three-frequency amplification in a lumped-element circuit [53]. Here three L–C resonators operating at signal, idler and pump angular frequencies ω_S, ω_I and ω_P are linked by a nonlinear capacitor C. The signal voltage is $V_S = \{v_S \exp(j\omega_S t) + \text{c.c.}\}/2$, where 'c.c.' denotes complex conjugate, and is taken from a source with output impedance R_{SO}. The pump voltage $V_P = \{v_P \exp(j\omega_P t) + \text{c.c.}\}/2$ is taken from a source with output impedance R_{P0} and the output from a load R_L. Because the idler is generated by a nonlinear interaction between the signal and pump, the relation $\omega_P = \omega_S + \omega_I$ can be assumed. The signal resonator contains a capacitor C_S and an inductor L_S with an associated resistance R_S. The idler and pump resonators are similar and their components are subscripted 'I' and 'P'. The nonlinear capacitor is assumed to respond as $C = C_1(1 + \beta V_C)$, where C_1 and β are constants and V_C is the voltage across C, which has a series resistance R_C. The current in each resonator is assumed only to contain terms oscillating near its resonance while the voltage across the nonlinear capacitor contains all three frequencies. Hence:

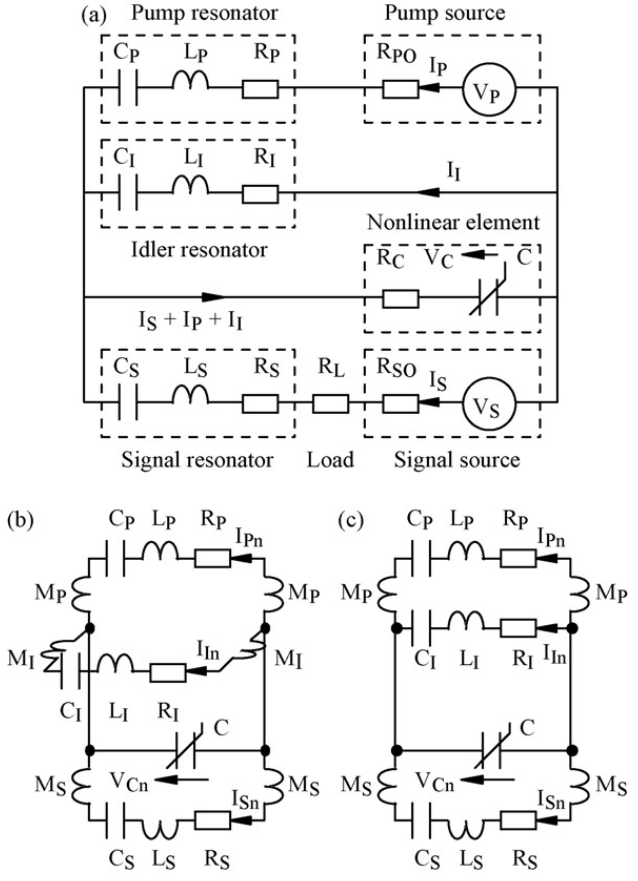

Fig. 3. (a) Three-frequency parametric amplifier; unit cell for amplification of MI waves (b) with and (c) without idler coupling.

$$
\begin{aligned}
I_S &= \frac{i_S \exp(j\omega_S t) + \text{c.c.}}{2} \\
I_I &= \frac{i_I \exp(j\omega_I t) + \text{c.c.}}{2} \\
I_P &= \frac{i_P \exp(j\omega_P t) + \text{c.c.}}{2} \\
V_C &= \frac{v_{CS} \exp(j\omega_S t) + \text{c.c.}}{2} + \frac{v_{CI} \exp(j\omega_I t) + \text{c.c.}}{2} \\
&\quad + \frac{v_{CP} \exp(j\omega_P t) + \text{c.c.}}{2}
\end{aligned}
\tag{6}
$$

Application of Kirchhoff's voltage law around each of the loops containing the nonlinear capacitor and neglect of unwanted terms yields:

$$
\begin{aligned}
&\left\{1 - \frac{\omega_{S0}^2}{\omega_S^2} - \frac{j}{Q_S}\right\} i_S + \frac{v_{CS}}{j\omega_S L_S} = \frac{v_S}{j\omega_S L_S} \\
&\left\{1 - \frac{\omega_{I0}^2}{\omega_I^2} - \frac{j}{Q_I}\right\} i_I + \frac{v_{CI}}{j\omega_I L_I} = 0 \\
&\left\{1 - \frac{\omega_{P0}^2}{\omega_P^2} - \frac{j}{Q_P}\right\} i_P + \frac{v_{CP}}{j\omega_P L_P} = \frac{v_P}{j\omega_P L_P}
\end{aligned}
\tag{7}
$$

Here $\omega_{S0}^2 = 1/L_S C_S$, $\omega_{I0}^2 = 1/L_I C_I$ and $\omega_{P0}^2 = 1/L_P C_P$ are nominal resonant frequencies for the signal, idler and pump resonators. Similarly, $Q_S = \omega_S L_S / R'_S$, $Q_I = \omega_I L_I / R'_I$ and $Q_P = \omega_P L_P / R'_P$ are the corresponding Q-factors, where $R'_S = R_S + R_C + R_{SO} + R_L$, $R'_I = R_I + R_C$ and $R'_P = R_P + R_C + R_{PO}$ are resistances around the three loops. For C itself, we have:

$$
I_{Sn} + I_{In} + I_{Pn} = \frac{d(CV_C)}{dt} = C_1(1 + 2\beta V_C)\frac{dV_C}{dt} \tag{8}
$$

Equating coefficients of $\exp(j\omega_S t)$, $\exp(j\omega_I t)$ and $\exp(j\omega_P t)$ separately, making use of the frequency relationship, and again ignoring unwanted terms, we obtain:

$$
\begin{aligned}
i_S &= j\omega_S C_1 \{v_{CS} + \beta v_{CI}^* v_{CP}\} \\
i_I &= j\omega_I C_1 \{v_{CI} + \beta v_{CS}^* v_{CP}\} \\
i_P &= j\omega_P C_1 \{v_{CP} + \beta v_{CS} v_{CI}\}
\end{aligned}
\tag{9}
$$

If the signal and idler are weak, the product $v_{CS} v_{CI}$ in the lowest of Eq. (9) may be neglected, so that $v_{CP} \approx i_P / j\omega_P C_1$. Substituting into the lower of Eq. (7),

we obtain:

$$\left[1-\frac{\omega'^2_{\mathrm{P0}}}{\omega_{\mathrm{P}}^2}-\frac{j}{Q'_{\mathrm{P}}}\right]i_{\mathrm{P}}=\frac{v_{\mathrm{P}}}{\mathrm{j}\omega_{\mathrm{P}}L_{\mathrm{P}}} \tag{10}$$

Here $\omega'^2_{\mathrm{P0}}=(1/L_{\mathrm{P}})\{1/C_{\mathrm{P}}+1/C_1\}$ is a modified pump resonant frequency, derived from the inductor L_{P} and the series sum of the capacitance C_{P} and the linear capacitance term C_1. If the pump frequency is such that $\omega_{\mathrm{P}}=\omega'_{\mathrm{P0}}$, we obtain $i_{\mathrm{P}}=v_{\mathrm{P}}/R'_{\mathrm{P}}$ and $v_{\mathrm{CP}}\approx v_{\mathrm{P}}/\mathrm{j}\omega_{\mathrm{P}}C_1R'_{\mathrm{P}}$. Considering now the signal and idler, the upper pair of Eq. (9) reduces to:

$$\begin{aligned}v_{\mathrm{CS}}&=\frac{i_{\mathrm{S}}\alpha}{\mathrm{j}\omega_{\mathrm{S}}C_1}-\frac{i_{\mathrm{I}}^*\alpha\beta v_{\mathrm{P}}}{\omega_{\mathrm{I}}\omega_{\mathrm{P}}C_1^2R'_{\mathrm{P}}}\\ v_{\mathrm{CI}}&=\frac{-i_{\mathrm{S}}^*\alpha\beta v_{\mathrm{P}}}{\omega_{\mathrm{S}}\omega_{\mathrm{P}}C_1^2R'_{\mathrm{P}}}+\frac{i_{\mathrm{I}}\alpha}{\mathrm{j}\omega_{\mathrm{I}}C_1}\end{aligned} \tag{11}$$

Here $\alpha=1/[1-\beta^2v_{\mathrm{CP}}v_{\mathrm{CP}}^*]$ is of order unity. The upper pair of Eq. (7) then becomes:

$$\begin{aligned}&\left\{1-\frac{\omega'^2_{\mathrm{S0}}}{\omega_{\mathrm{S}}^2}-\frac{j}{Q_{\mathrm{S}}}\right\}i_{\mathrm{S}}-\frac{i_{\mathrm{I}}^*\alpha\beta v_{\mathrm{P}}}{\mathrm{j}\omega_{\mathrm{S}}\omega_{\mathrm{I}}\omega_{\mathrm{P}}L_{\mathrm{S}}C_1^2R'_{\mathrm{P}}}=\frac{v_{\mathrm{S}}}{\mathrm{j}\omega_{\mathrm{S}}L_{\mathrm{S}}}\\ &\left\{1-\frac{\omega'^2_{\mathrm{I0}}}{\omega_{\mathrm{I}}^2}-\frac{j}{Q_{\mathrm{I}}}\right\}i_{\mathrm{I}}-\frac{i_{\mathrm{S}}^*\beta v_{\mathrm{P}}}{\mathrm{j}\omega_{\mathrm{S}}\omega_{\mathrm{I}}\omega_{\mathrm{P}}L_{\mathrm{I}}C_1^2R'_{\mathrm{P}}}=0\end{aligned} \tag{12}$$

Here $\omega'^2_{\mathrm{S0}}=(1/L_{\mathrm{S}})\ \{1/C_{\mathrm{S}}+\alpha/C_1\}$ is a modified signal resonant frequency, and $\omega'^2_{\mathrm{I0}}=(1/L_{\mathrm{I}})\ \{1/C_{\mathrm{I}}+\alpha/C_1\}$ is a similar term for the idler. If the signal and idler frequencies are correctly chosen we can have $\omega_{\mathrm{S}}=\omega'_{\mathrm{S0}}$ and $\omega_{\mathrm{I}}=\omega'_{\mathrm{I0}}$ and hence

$$\begin{aligned}i_{\mathrm{I}}&=\frac{i_{\mathrm{S}}^*\alpha\beta v_{\mathrm{P}}}{\omega'_{\mathrm{S0}}\omega'_{\mathrm{P0}}C_1^2R'_{\mathrm{I}}R'_{\mathrm{P}}}\\ i_{\mathrm{S}}&=\frac{v_{\mathrm{S}}}{R'_{\mathrm{Seff}}}\end{aligned} \tag{13}$$

Where R'_{Seff} is an effective signal resistance, given by:

$$R'_{\mathrm{Seff}}=R'_{\mathrm{S}}-R_{\mathrm{A}},\quad \text{where } R_{\mathrm{A}}=\frac{\alpha^2\beta^2v_{\mathrm{P}}v_{\mathrm{P}}^*}{\omega'_{\mathrm{S0}}\omega'_{\mathrm{I0}}\omega'^2_{\mathrm{P0}}C_1^4R'_{\mathrm{I}}R'^2_{\mathrm{P}}} \tag{14}$$

The amplifier is therefore a negative resistance type, which uses the power of the pump to decrease the effective resistance of the signal circuit and increase its Q-factor. The voltage dropped across R_{L} is $i_{\mathrm{S}}R_{\mathrm{L}}$, so the voltage gain is $G=R'_{\mathrm{S}}/(R'_{\mathrm{S}}-R_{\mathrm{A}})$. Because the effect is determined by $v_{\mathrm{P}}v_{\mathrm{P}}^*$, there is no dependence on pump phase. However, low overall idler and pump resistances are required to achieve a significant effect at low pump powers. Furthermore, at high pump powers and high gains, the amplification is sensitive to small changes in the resonant frequencies caused by the term α and to frequency variations, and if the device is pumped sufficiently hard that $R_{\mathrm{A}}=R'_{\mathrm{S}}$, self-oscillation will occur.

4. Parametric amplification of magneto-inductive waves

We now consider how the three-frequency amplifier might be adapted for MI waves. Fig. 3b shows a unit cell that might offer one approach. Here the signal, idler and pump loops in Fig. 3a are provided with mutual inductances M_{S}, M_{I} and M_{P} that allow nearest-neighbour magnetic coupling when a set of cells are arranged in an array. This arrangement will clearly allow propagation of signal, idler and pump as separate MI waves, which are linked by nonlinear capacitances. Note that the signal and pump sources have been omitted, together with the load and the varactor resistance. Analysis can proceed as before. If the signal, pump and idler currents in the nth section are labelled $I_{\mathrm{S}n}$, $I_{\mathrm{I}n}$ and $I_{\mathrm{P}n}$ and the voltages across the nonlinear capacitor at the three frequencies are labelled $v_{\mathrm{CS}n}$, $v_{\mathrm{CI}n}$ and $v_{\mathrm{CP}n}$, Kirchhoff's law gives:

$$\begin{aligned}&\left\{1-\frac{\omega_{\mathrm{S0}}^2}{\omega_{\mathrm{S}}^2}-\frac{j}{Q_{\mathrm{S}}}\right\}i_{\mathrm{S}n}\\ &\quad+(\kappa_{\mathrm{S}}/2)\{i_{\mathrm{S}n-1}+i_{\mathrm{S}n+1}\}+\frac{v_{\mathrm{CS}n}}{\mathrm{j}\omega_{\mathrm{S}}L_{\mathrm{S}}}=0\\ &\left\{1-\frac{\omega_{\mathrm{I0}}^2}{\omega_{\mathrm{I}}^2}-\frac{j}{Q_{\mathrm{I}}}\right\}i_{\mathrm{I}n}\\ &\quad+(\kappa_{\mathrm{I}}/2)\{i_{\mathrm{I}n-1}+i_{\mathrm{I}n+1}\}+\frac{v_{\mathrm{CI}n}}{\mathrm{j}\omega_{\mathrm{I}}L_{\mathrm{I}}}=0\\ &\left\{1-\frac{\omega_{\mathrm{P0}}^2}{\omega_{\mathrm{P}}^2}-\frac{j}{Q_{\mathrm{P}}}\right\}i_{\mathrm{P}n}\\ &\quad+(\kappa_{\mathrm{P}}/2)\{i_{\mathrm{P}n-1}+i_{\mathrm{P}n+1}\}+\frac{v_{\mathrm{CP}n}}{\mathrm{j}\omega_{\mathrm{P}}L_{\mathrm{P}}}=0\end{aligned} \tag{15}$$

Here $\kappa_{\mathrm{S}}=2M_{\mathrm{S}}/L_{\mathrm{S}}$, $\kappa_{\mathrm{I}}=2M_{\mathrm{I}}/L_{\mathrm{I}}$ and $\kappa_{\mathrm{P}}=2M_{\mathrm{P}}/L_{\mathrm{P}}$ are the coupling coefficients for the signal, idler and pump. Similarly, for the nonlinear capacitor we now have:

$$\begin{aligned}i_{\mathrm{S}n}&=\mathrm{j}\omega_{\mathrm{S}}C_1\{v_{\mathrm{CS}n}+\beta v_{\mathrm{CI}n}^*v_{\mathrm{CP}n}\}\\ i_{\mathrm{I}n}&=\mathrm{j}\omega_{\mathrm{I}}C_1\{v_{\mathrm{CI}n}+\beta v_{\mathrm{CS}n}^*v_{\mathrm{CP}n}\}\\ i_{\mathrm{P}n}&=\mathrm{j}\omega_{\mathrm{P}}C_1\{v_{\mathrm{CP}n}+\beta v_{\mathrm{CS}n}v_{\mathrm{CI}n}\}\end{aligned} \tag{16}$$

If the signal and idler waves are weak compared with the pump, the voltage product in the lowest of Eq. (16) may be neglected as before, so that $v_{\mathrm{CP}n}\approx i_{\mathrm{P}n}/\mathrm{j}\omega_{\mathrm{P}}C_1$. Substituting into the lowest of Eq. (15), we obtain a

recurrence equation for the pump currents:

$$\left\{1-\frac{\omega'^2_{P0}}{\omega_P^2}-\frac{j}{Q_P}\right\}i_{Pn}+\left(\frac{\kappa_P}{2}\right)\{i_{Pn-1}+i_{Pn+1}\}=0 \tag{17}$$

Eq. (17) implies that the pump simply propagates as a magneto-inductive wave. Considering now the signal and idler, the upper pair of Eq. (15) reduces to:

$$\begin{aligned} v_{CSn} &= \frac{i_{Sn}\alpha}{j\omega_S C_1}-\frac{i_{In}^*\alpha\beta i_{Pn}}{\omega_I\omega_P C_1^2} \\ v_{CIn} &= -\frac{i_{Sn}^*\alpha\beta i_{Pn}}{\omega_S\omega_P C_1^2}+\frac{i_{In}\alpha}{j\omega_I C_1} \end{aligned} \tag{18}$$

Substituting into the upper pair of Eq. (15) we then get:

$$\begin{aligned} &\left\{1-\frac{\omega'^2_{S0}}{\omega_S^2}-\frac{j}{Q_S}\right\}i_{Sn} \\ &\quad+(\kappa_S/2)\{i_{Sn-1}+i_{Sn+1}\}-\frac{i_{In}^*\alpha\beta i_{Pn}}{j\omega_S\omega_I\omega_P L_S C_1^2}=0 \\ &\left\{1-\frac{\omega'^2_{I0}}{\omega_I^2}-\frac{j}{Q_I}\right\}i_{In} \\ &\quad+(\kappa_I/2)\{i_{In-1}+i_{In+1}\}-\frac{i_{Sn}^*\alpha\beta i_{Pn}}{j\omega_S\omega_I\omega_P L_I C_1^2}=0 \end{aligned} \tag{19}$$

Eq. (19) can of course be recast as iteration relations, allowing (for example) i_{Sn+1} and i_{In+1} to be found in terms of i_{Sn}, i_{In}, i_{Pn}, i_{Sn-1} and i_{In-1} under any conditions. Here, however, we briefly examine a simpler solution. If we assume the signal, idler and pump currents are travelling waves in the form $i_{Sn}=i_S\exp(-jk_S na)$, $i_{In}=i_I\exp(-jk_I na)$ and $i_{Pn}=i_P\exp(-jk_P na)$ where i_S, i_I and i_P are amplitudes and k_S, k_I and k_P are propagation constants, we obtain:

$$\begin{aligned} &\left[\left\{1-\frac{\omega'^2_{S0}}{\omega_S^2}-\frac{j}{Q_S}\right\}+\kappa_S\cos(k_S a)\right]i_S \\ &\quad-\frac{i_I^*\alpha\beta i_P\exp\{j(k_S+k_I-k_P)na\}}{j\omega_S\omega_I\omega_P L_S C_1^2}=0 \\ &\left[\left\{1-\frac{\omega'^2_{I0}}{\omega_I^2}-\frac{j}{Q_I}\right\}+\kappa_I\cos(k_I a)\right]i_I \\ &\quad-\frac{i_S^*\alpha\beta i_P\exp\{j(k_S+k_I-k_P)na\}}{j\omega_S\omega_I\omega_P L_I C_1^2}=0 \end{aligned} \tag{20}$$

The exponentials vanish if $k_P=k_S+k_I$—the phase matching condition for a three-frequency travelling wave amplifier [59]. If this condition holds, and there is also no loss, we get:

$$\begin{aligned} &\left[\left\{1-\frac{\omega'^2_{S0}}{\omega_S^2}\right\}+\kappa_S\cos(k_S a)\right]i_S-\frac{i_I^*\alpha\beta i_P}{j\omega_S\omega_I\omega_P L_S C_1^2}=0 \\ &\left[\left\{1-\frac{\omega'^2_{I0}}{\omega_I^2}\right\}+\kappa_I\cos(k_I a)\right]i_I-\frac{i_S^*\alpha\beta i_P}{j\omega_S\omega_I\omega_P L_I C_1^2}=0 \end{aligned} \tag{21}$$

Uncoupling Eq. (21) we then get

$$\begin{aligned} &\left[\left\{1-\frac{\omega'^2_{S0}}{\omega_S^2}\right\}+\kappa_S\cos(k_S a)\right] \\ &\quad\times\left[\left\{1-\frac{\omega'^2_{I0}}{\omega_I^2}\right\}+\kappa_I\cos(k_I a)\right]-\gamma^2=0 \end{aligned} \tag{22}$$

Here $\gamma^2=\alpha^2\beta^2 i_P i_P^*/\omega_S^2\omega_I^2\omega_I^2 L_I L_P C_1^4$. To solve Eq. (21), we assume that $k_S=k_{S0}+\Delta k_S$ and $k_I=k_{I0}-\Delta k_S$, where k_{S0} and k_{I0} are the propagation constants obtained in the absence of pumping ($\gamma=0$). Assuming that Δk_S is small, and eliminating terms using the dispersion equations of the signal and idler waves in the absence of pumping, we get:

$$\Delta k_S=\pm\frac{j\gamma}{\{\kappa_S\kappa_I\sin(k_{S0}a)\sin(k_{I0}a)\}^{1/2}} \tag{23}$$

Because Δk_S is imaginary, Eq. (23) describes a gain coefficient for exponential growth of the signal and idler, the conventional result. Here we have implicitly assumed that κ_S and κ_I have the same sign, so that the group velocities of the two waves are in the same direction. Loss and lack of phase matching both complicate the analysis, and it is not our purpose to present further details here. We simply point out that the results obtained so far for MI waves are entirely analogous to those of Tien [59], to show how they relate to earlier work.

Instead, we note that the conditions $\omega_P=\omega_S+\omega_I$ and $k_P=k_S+k_I$ will be difficult to satisfy using waves with complicated dispersion characteristics, and even more so in a ring geometry in which the three waves must be simultaneously resonant. To relax these constraints, we return to Eq. (19), and consider the case when the idler resonators are uncoupled as shown in Fig. 2c, so that $\kappa_I=0$. Now, the lower equation becomes:

$$i_{In}=\frac{i_{Sn}^*\alpha\beta i_{Pn}}{j\omega_S\omega_I\omega_P L_I C_1^2\{1-(\omega'^2_{I0}/\omega_I^2)-(j/Q_I)\}} \tag{24}$$

Assuming now that the idler matches its resonance, so that $\omega_I^2=\omega'^2_{I0}$, the idler currents are simply given by $i_{In}=i_{Sn}^*\alpha\beta i_{Pn}/\omega_S\omega_P R_I' C_1^2$ and the upper Eq. (19)

reduces to:

$$\left\{1-\frac{\omega'^2_{S0}}{\omega_S^2}-\frac{j}{Q_{Seff}}\right\} i_{Sn}+\left(\frac{\kappa_S}{2}\right)\{i_{Sn-1}+i_{Sn+1}\}=0 \tag{25}$$

Here the effective Q-factor of the signal resonators is now $Q_{Seff}=\omega_S L_S/R'_{Seff}$, where:

$$R'_{Seff}=R'_S-R_B, \quad \text{where } R_B=\frac{\alpha^2\beta^2 i_{Pn}i^*_{Pn}}{\omega'_S\omega'_{I0}\omega'^2_P C_1^4 R'_I} \tag{26}$$

Eq. (25) is again a recurrence equation for a magneto-inductive wave. Eq. (26) implies that the effective Q-factor of the signal resonators must rise as $i_{Pn}i^*_{Pn}$ increases, and Eq. (2) then implies that MI wave propagation losses must reduce. The overall system therefore again corresponds to a travelling wave negative resistance amplifier, albeit with slightly different characteristics to the conventional design.

The requirement that $\omega_I=\omega'_{I0}$ clearly renders the arrangement in Fig. 3c less versatile than the one in Fig. 3b, in which the idler can exist over a band. However, in the case of a ring resonator in a MRI application where bandwidths are small, it offers some advantages. The signal and pump need merely be resonant on suitable ring modes, and the idler operating on its resonant frequency. Because the effect is determined by $i_{Pn}i^*_{Pn}$, there is again no dependence on pump phase. There is no requirement for phase matching, and the group velocities of the pump and signal waves need not even have the same sign.

5. Experimental verification

Experimental verification of the ideas of the previous section is not straightforward. The MRI application requires construction of a ring with suitable size, operating on a specified frequency (for example, 63.8 MHz for ^{1}H MRI in a 1.5 T field), using non-magnetic components. However, several non-ideal effects can be anticipated. The nearest-neighbour coupling needed for MI waves will inevitably be accompanied by coupling between non-nearest-neighbours and between the three sets of resonators. Provision of the low-impedance sources and loads needed for high Q-factors is difficult, given standardisation on 50 Ω systems. Weak inductive probes can be used for input and output coupling, but will lead to coupling between the pump and signal source and the detector, resulting in poor SNR and an inaccurate gain figure. Compromises were therefore required. A scaled-down test-bed operating in the correct frequency band was constructed, using as few magnetic components as possible, with the intention of following the demonstration of amplification with a more realistic system. Strong nearest-neighbour coupling was obtained using closely spaced air-cored rectangular inductors. There is little to be done about non-nearest-neighbour coupling; however, coupling between the signal and pump lines was minimised by separating the two with the idlers, which were based on compact, cored inductors.

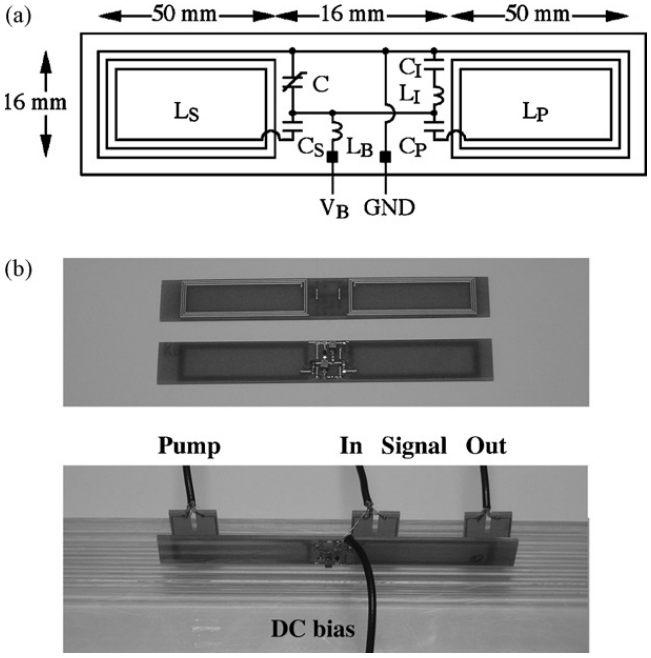

Fig. 4. (a) Layout of amplifier unit cell; (b) prototype unit cell and arrangement for amplification.

5.1. Electrical components

Experiments were carried out using FR-4 PCB unit cells with the layout of Fig. 4a. The inductors L_S and L_P were three-turn spirals formed from 85 μm thick Cu with 1 mm wide tracks and 0.5 mm separations, designed with rectangular shape to provide strong nearest-neighbour coupling between elements placed edge-to-edge. The PCB inductors had a good Q-factor (110 at 80 MHz), but a significant parasitic capacitance (3.3 pF), which necessitated careful choice of components to ensure that the idler and the pump and signal bands were appropriately separated. The inductors L_I and the capacitors C_S, C_I and C_P were surface-mount components. The nonlinear capacitors were Philips BB149A RF varactor diodes, with a reverse bias applied using inductors L_B. Fig. 4b shows a unit cell.

Table 1
Component values for unit cells and rings

	L_B (μH)	L_S (μH)	C_S (pF)	L_I (μH)	C_I (pF)	L_P (μH)	C_P (pF)
Unit cell	4.7	0.68	330	4.7	3.3	0.68	10
Ring	4.7	0.68	330	4.7	10.0	0.68	10

The varactor capacitance varies with reverse voltage V approximately as [76]:

$$C \approx \frac{C_{10}}{(1 + V/V_{bi})^{0.5}} \quad (27)$$

Here $C_{10} \approx 22$ pF and $V_{bi} \approx 0.9$ V. Assuming that V is the sum of a dc bias V_B and an ac voltage V_C, where V_C is small, we obtain $C = C_1(1 + \beta V_C)$, with:

$$C_1 = \frac{C_{10}}{(1 + V_B/V_{bi})^{0.5}} \quad \text{and} \quad \beta = -\frac{1}{2(V_{bi} + V_B)} \quad (28)$$

The effect of the term C_1 on the resonant frequencies f'_{S0}, f'_{I0} and f'_{P0} (corresponding to the angular frequencies ω'_{S0}, ω'_{I0} and ω'_{P0}, respectively) will be significant if C_S, C_I and C_P are large compared with C_1. Since the resonances will all then depend on V_B, it is preferable to choose C_S and C_I so that f'_{S0} and f'_{I0} are approximately fixed, while f'_{P0} can be varied to satisfy the relation $f'_{P0} = f'_{S0} + f'_{I0}$. However, since the nonlinear coefficient β declines as V_B increases, it is important that matching is achieved at a V_B that is small, but not so small that the diode is driven into conduction when pumped. Component values were as shown in Table 1; these gave resonant frequencies $f'_{I0} \approx 30$ MHz, $f'_{S0} \approx 40$ MHz and $f'_{P0} \approx 70$ MHz.

5.2. Unit cells

Characterisation was carried out using an Agilent E5061A network analyser. The voltage dependence of the signal, idler and pump resonances was first established, by weak coupling using small PCB inductors, as shown in Fig. 4b. This approach avoided degradation of the Q-factor of the signal resonator. Fig. 5a shows the frequency variation of S_{21} at different V_B and Fig. 5b the voltage dependence of f'_{S0}, f'_{I0} and f'_{P0}. These results imply that the signal and idler resonances are relatively constant. However, the pump resonance increased quasi-linearly with V_B, allowing frequency matching at $V_B \approx 3$ V. Weak coupling was then used to couple a HP 8647A source into the pump resonator, via a 17 dB Farnell LA1000 RF power amplifier. Fig. 6a shows the frequency variation of S_{21} at $V_B = 3$ V, with and without pumping at 23 dB m. Pumping increases the Q-factors of the idler and signal, and causes small shifts in resonance to lower frequencies. However, there is significant breakthrough of the pump. To measure the gain, a second HP 8647A source was coupled into the signal resonator and the amplified signal observed on the network analyser at the signal frequency. Fig. 6b shows the variation in gain with pump power, showing a gain of >20 dB. However, care was required to prevent oscillation at high gains.

5.3. Ring resonators

MI waveguides were constructed with edge-coupled cells as shown in Fig. 7a, using connecting wires to distribute the ground and bias. Coupling coefficients were established by the split resonance method [10,11], giving the values shown in Table 2. The values of κ_1 and Q corre-

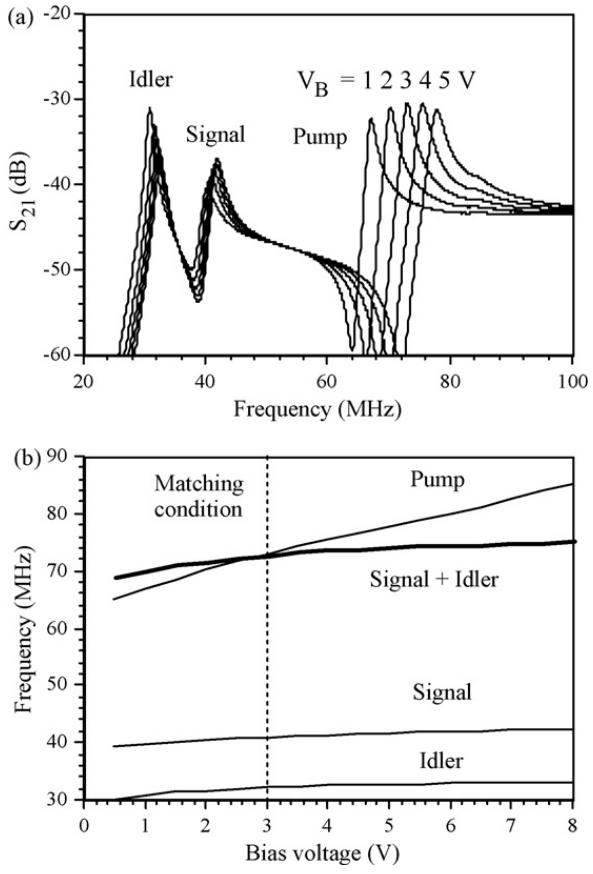

Fig. 5. (a) Transfer characteristics of inductively probed unit cell at different V_B; (b) voltage dependence of signal, idler and pump resonances.

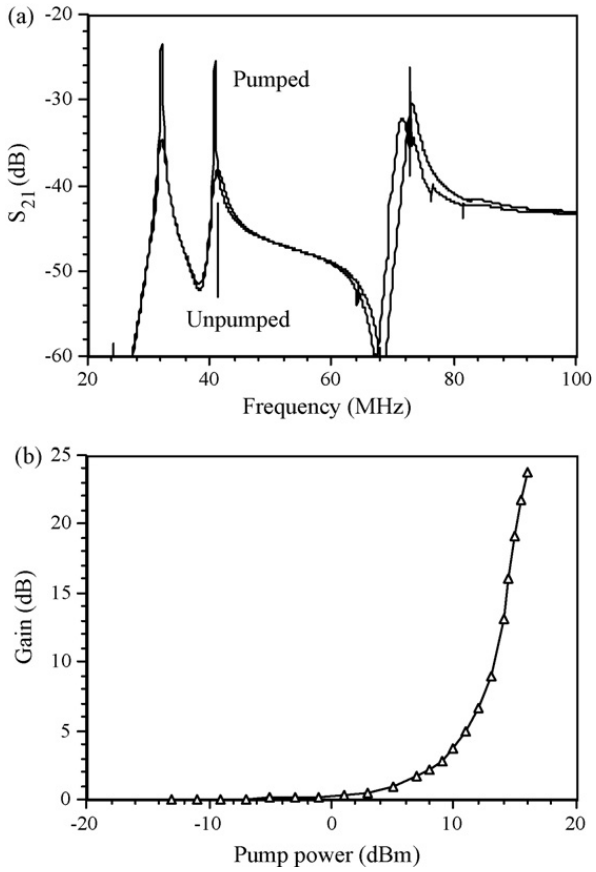

Fig. 6. (a) Transfer characteristics of unit cell, without and with pump applied; (b) variation of gain with pump power.

spond to loss of ≈0.15 dB/element at mid-band. Similar coefficients were obtained for the signal and pump. As expected, significant coupling between non-nearest-neighbours was found, with $\kappa_2/\kappa_1 \approx 1/9$, the value used to generate the dashed line theoretical dispersion curve in Fig. 2b. Coupling was also found between the signal and the pump waveguide; this coefficient is positive because of the definition of the current directions. As a result, resonant frequencies altered and it was necessary to increase C_I and reduce the idler frequency to around 20 MHz, to prevent the idler overlapping the signal band. A 16-element polygonal ring was constructed by inserting cells into Perspex baseboards carrying grooves formed by CNC machining. Fig. 7b shows the complete ring with an inductively coupled input and output for the signal on either side of a diameter. The pump was applied in a similar way, using additional probes.

Table 2
Coupling coefficients for the most significant interactions

	κ_1	κ_2
Signal–signal	−0.3	−0.035
Signal–pump	+0.055	

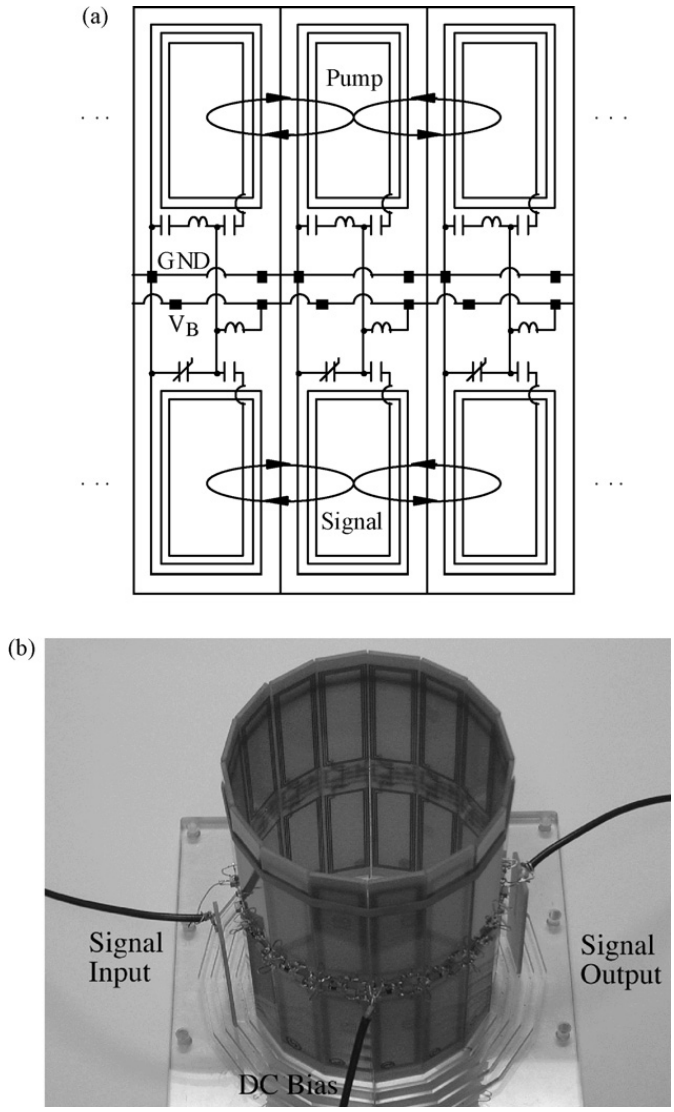

Fig. 7. (a) Arrangement for travelling wave amplification; (b) prototype 16-element ring.

The voltage dependence of the different resonances was again established first. Fig. 8a shows the frequency variation of S_{11} and S_{21} for $V_B = 2$ V. The individual signal and pump resonances of Fig. 5a have now both separated into a set of resonances at frequencies $f'_{S\mu}$ and $f'_{P\mu}$, confirming that the signal and pump are both propagating as waves. No band was observed for the idler. Losses were low enough to identify all except the lowest frequency resonances ($\mu = 8$, which is close to $\mu = 7$) unambiguously. Fig. 8b shows the mode frequencies as a dispersion diagram, for different V_B. The signal and pump have similar dispersion, as might be expected from their near-identical coupling arrangements. In each case, the dispersion diagram is distorted from the simplest example in Fig. 2a, due to non-nearest-neighbour coupling. The pump modes are more sensitive to changes in V_B.

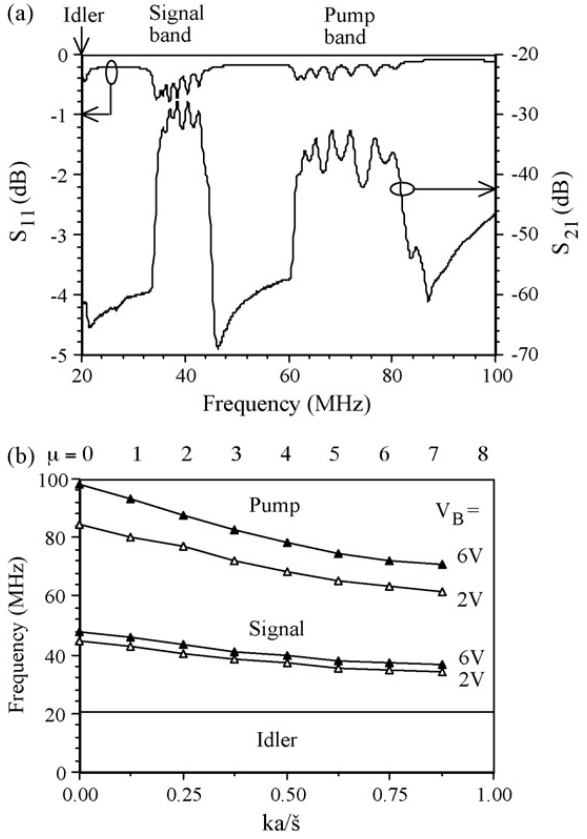

Fig. 8. (a) Transfer characteristic and (b) dispersion characteristic of inductively probed ring.

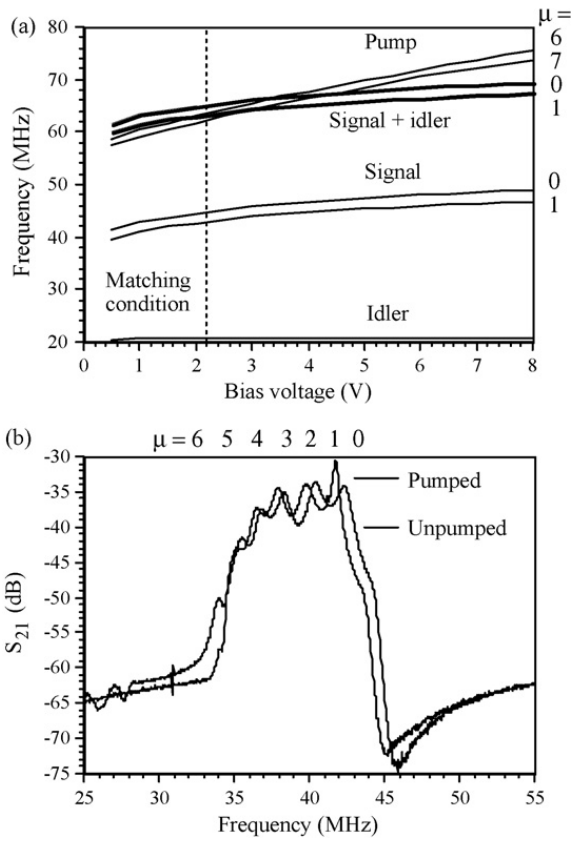

Fig. 9. (a) Voltage dependence of signal, idler and pump resonances; (b) transfer characteristics of ring, without and with pumping by the 6th pump mode to amplify the 1st signal mode.

Fig. 9a shows the variation with V_B of the lowest order signal and highest order pump resonances. These results show that frequency matching may be achieved for several pairs of resonances at different V_B, in the useful range of a few Volts. In particular, it was possible to match the primary signal mode with the sixth pump mode at $V_B \approx 2$ V. Fig. 9b shows the variation of S_{21} over the signal band, without and with pumping at 21 dB m at f'_{P6}. Amplification of ≈5 dB at f'_{S1} may be seen, demonstrating a transfer of energy from the pump band to the signal band. This figure is lower than the gain for single elements, but respectable given the complexity of the circuit.

Similar gains were achieved when the pump was applied at the signal input and at the output, suggesting that the pump direction is unimportant. Similar gain was also achieved at lower power when the pump was applied at both locations, suggesting that pump loss is significant. Gain was also achieved at the signal frequency f'_{S0}, which may also be coupled to the sixth pump mode. By component adjustment, it is likely that further matching may be achieved, so that (for example) the primary signal mode might be amplified by a lower loss pump mode near the band centre.

6. Discussion

Parametric amplification of magneto-inductive waves propagating in coupled chains of nonlinear *L–C* resonators has been studied theoretically and experimentally. Analysis has been presented for a three-frequency travelling wave scheme in which the signal, idler and pump all propagate as MI waves. Nearest-neighbour coupling has been assumed, but it is relatively simple to incorporate non-nearest-neighbour coupling between elements of the same line following the method in [11], for example as in Eq. (3). The major result is a distortion of the dispersion characteristic, as indicated in Fig. 2b. De-coupling the idler resonators has been shown to relax the standard phase matching condition, making it relatively simple to investigate alternative pumping configurations.

Confirmation of the theory has been provided using low-frequency printed circuit board unit cells containing varactor diodes, arranged as a 16-element polygonal ring resonator. Frequency matching and selective amplification of the primary resonance has been demonstrated. Currently the main limitations are losses and unwanted

mutual interactions between the pump and signal lines. Because of the lack of sensitivity to pump phase, the latter could be overcome by avoiding the use of a MI wave to distribute the pump, for example by using a co-axial line. Such a modification would in turn greatly reduce pump noise. Alternatively, the pump wave could be propagated on an axial MI waveguide rather than a planar waveguide. In this case, nearby unit cells of the signal and pump waveguides would be approximately orthogonal and hence weakly coupled. These alternatives will be considered in future investigations. The primary resonance can be excited by a rotating magnetic dipole in magnetic resonance imaging. Future work will involve improvement of the gain and signal to noise ratio, elimination of all remaining magnetic materials and tuning to a suitable frequency for MRI experiments.

Acknowledgements

The Authors are grateful to EPSRC for financial support under grant EP/D048389/1, to Mr. Philip Jones for constructing the CNC machined baseboards and to Dr. Ekaterina Shamonina and Dr. Oleksiy Sydoruk of Osnabrück University for valuable discussions.

References

[1] V.G. Veselago, The electrodynamics of substances with simultaneously negative values of ε and μ, Sov. Phys. Usp. 10 (1968) 509–514.
[2] J.B. Pendry, A.J. Holden, D.J. Robbins, W.J. Stewart, Magnetism from conductors and enhanced nonlinear phenomena, IEEE Trans Micro. Theor. Tech. MTT 47 (1999) 2075–2084.
[3] E. Shamonina, V.A. Kalinin, K.H. Ringhofer, L. Solymar, Magneto-inductive waveguide, Elect. Lett. 38 (2002) 371–373.
[4] E. Shamonina, V.A. Kalinin, K.H. Ringhofer, L. Solymar, Magnetoinductive waves in one, two, and three dimensions, J. Appl. Phys. 92 (2002) 6252–6261.
[5] R.R.A. Syms, E. Shamonina, L. Solymar, Positive and negative refraction of magnetoinductive waves in two dimensions, Eur. Phys. J. B 46 (2005) 301–308.
[6] R.R.A. Syms, E. Shamonina, V. Kalinin, L. Solymar, A theory of metamaterials based on periodically loaded transmission lines: interaction between magneto-inductive and electro-magnetic waves, J. Appl. Phys. 97 (2005) 064909.
[7] O. Zhuromskyy, E. Shamonina, L. Solymar, Effect of radiation on dispersion of magneto-inductive waves in a metamaterial, Proc. SPIE 5955 (2005) 06-1–06-8.
[8] M.C.K. Wiltshire, E. Shamonina, I.R. Young, L. Solymar, Dispersion characteristics of magneto-inductive waves: comparison between theory and experiment, Elect. Lett. 39 (2003) 215–217.
[9] E. Shamonina, L. Solymar, Magneto-inductive waves supported by metamaterial elements: components for a one-dimensional waveguide, J. Phys. D: Appl. Phys. 37 (2004) 362–367.
[10] R.R.A. Syms, I.R. Young, L. Solymar, Low-loss magneto-inductive waveguides, J. Phys. D: Appl. Phys. 39 (2006) 3945–3951.
[11] R.R.A. Syms, O. Sydoruk, E. Shamonina, L. Solymar, Higher order interactions in magneto-inductive waveguides, Metamaterials 1 (2007) 44–51.
[12] A. Radkovskaya, M. Shamonin, C.J. Stevens, G. Faulkner, D.J. Edwards, E. Shamonina, L. Solymar, An experimental study of the properties of magnetoinductive waves in the presence of retardation, J. Magn. Magn. Mat. 300 (2006) 29–32.
[13] M.C.K. Wiltshire, E. Shamonina, I.R. Young, L. Solymar, Experimental and theoretical study of magneto-inductive waves supported by one-dimensional arrays of "swiss rolls, J. Appl. Phys. 95 (2004) 4488–4493.
[14] R.R.A. Syms, E. Shamonina, Solymar L, Magneto-inductive waveguide devices, IEE Proc. Micro. Ant. Prop. 153 (2006) 111–121.
[15] M.J. Freire, R. Marques, F. Medina, M.A.G. Laso, F. Martin, Planar magneto-inductive wave transducers: Theory and applications, Appl. Phys. Lett. 85 (2004) 4439–4441.
[16] I.S. Nefedov, S.A. Tretyakov, On potential applications of metamaterials for the design of broadband phase shifters, Micro. Opt. Tech. Lett. 145 (2005) 98–102.
[17] L. Solymar, O. Zhuromskyy, O. Sydoruk, E. Shamonina, I.R. Young, R.R.A. Syms, Rotational resonance of magnetoinductive waves: basic concept and application to nuclear magnetic resonance, J. Appl. Phys. 99 (2006) 123908.
[18] M.J. Freire, R. Marques, A planar magneto-inductive lens for 3D subwavelength imaging, Appl. Phys. Lett. 86 (2005) 182505-1-3.
[19] O. Sydoruk, M. Shamonin, A. Radkovskaya, O. Zhuromskyy, E. Shamonona, R. Trautner, C.J. Stevens, G. Faulkner, D.J. Edwards, L. Solymar, Mechanism of subwavelength imaging with bilayered magnetic metamaterials: theory and experiment, J. Appl. Phys. 101 (2007) 073903.
[20] O. Sydoruk, E. Shamonina, L. Solymar, Parametric amplification in coupled magnetoinductive waveguides, J. Phys. D: Appl. Phys. 40 (2007) 6879–6887.
[21] J. Shefer, Periodic cylinder arrays as transmission lines, IEEE Trans. Micro. Theor. Tech. 11 (1963) 55–61.
[22] C.C. Lee, L.C. Shen, Travelling waves in coupled Yagi structures, IEEE Trans. Micro. Theor. Tech. 25 (1977) 931–933.
[23] S.A. Tretyakov, A.J. Viitanen, Line of periodically arranged passive dipole scatterers, Elect. Eng. 82 (2000) 353–361.
[24] R.A. Silin, Dispersion characteristics of 2D and 3D periodic systems (artificial dielectrics), RadioTekh. Elektron. 5 (1960) 688–691 (in Russian).
[25] J.S. Hong, M.J. Lancaster, Coupling of microstrip square open-loop resonators for cross-coupled planar microwave filters, IEEE Trans. Micro. Theor. Tech. 44 (1996) 2099–2109.
[26] D.R. Smith, W.J. Padilla, D.C. Vier, S.C. Nemat-Nasser, S. Schultz, Composite medium with simultaneously negative permeability and permittivity, Phys. Rev. Lett. 84 (2000) 4184–4187.
[27] R.A. Shelby, D.R. Smith, S.C. Nemat-Nasser, S. Schultz, Microwave transmission through a two-dimensional isotropic left-handed metamaterial, Appl. Phys. Lett. 78 (2001)489–491.
[28] R. Marques, F. Mesa, J. Martel, F. Medina, Comparative analysis of edge- and broadside-coupled split ring resonators for metamaterial design—theory and experiments, IEEE Trans. Anten. Prop. 51 (2003) 2572–2581.

[29] A. Yariv, Y. Xu, R.K. Lee, A. Scherer, Coupled resonator optical waveguide: a proposal and analysis, Opt. Lett. 24 (1999) 711–713.
[30] I. Gil, J. Bonache, J. García-García, F. Martin, Tunable metamaterial transmission lines based on varactor loaded split-ring resonators, IEEE Trans. MTT 54 (2006) 2665–2674.
[31] I.V. Shadrivov, S.K. Morrison, Y.S. Kivshar, Tunable split-ring resonators for nonlinear negative-index metamaterials, Opt. Exp. 14 (2006) 9344–9349.
[32] D. Kuylenstierna, A. Vorobiev, P. Linner, S. Gevorgian, Composite right/left handed transmission line phaseshifter using ferroelectric varactors, IEEE Micro. Wireless Comp. Lett. 16 (2006) 167–169.
[33] A. Zharov, I.V. Shadrivov, Y.S. Kivshar, Nonlinear properties of left-handed metamaterials, Phys. Rev. Lett. 91 (2003) 037401.
[34] M. Lapine, M. Gorkunov, K.H. Ringhofer, Nonlinearity of a metamaterial arising from diode insertions into resonant conductive elements, Phys. Rev. E 67 (2003) 065601.
[35] M. Lapine, M. Gorkunov, Three-wave coupling of microwaves in metamaterials with nonlinear resonant conductive elements, Phys. Rev. E 70 (2004) 66601.
[36] A.B. Kozyrev, H. Kim, A. Karbassi, D.W. van der Weide, Wave propagation in nonlinear left-handed transmission line media, Appl. Phys. Lett. 87 (2005) 121109.
[37] A.B. Kozyrev, H. Kim, D.W. van der Weide, Parametric amplification in left-handed transmission line media, Appl. Phys. Lett. 88 (2006) 264101.
[38] L. Brillouin, Wave Propagation in Periodic Structures, McGraw-Hill Book Co. Ltd., New York, 1946.
[39] M. Rahman, M.A. Stuchly, Transmission line-periodic circuit representation of planar microwave photonic bandgap structures, Micro. Opt. Tech. Lett. 30 (2001) 15–19.
[40] G.V. Eleftheriades, A.K. Iyer, P.C. Kremer, Planar negative refractive index media using periodically *L–C* loaded transmission lines, IEEE Trans. Micro. Theor. Tech. 50 (2002) 2702–2712.
[41] A. Grbic, G.V. Eleftheriades, Periodic analysis of a 2-D negative refractive index transmission line structure, IEEE Trans. Antan. Prop. 51 (2003) 2604–2611.
[42] J.M. Manley, H.E. Rowe, Some general properties of nonlinear elements—Part I. General energy relations, Proc. IRE 44 (1956) 904–913.
[43] H.E. Rowe, Some general properties of nonlinear elements – Part II. Small signal theory, Proc. IRE 46 (1958) 850–860.
[44] W.W. Mumford, Some notes on the history of parametric transducers, Proc. IRE 48 (1960) 848–853.
[45] K.K.N. Chang, S. Bloom, Theory of parametric amplifiers, RCA Rev. 18 (1957) 578–593.
[46] G.A. Klotzbaugh, Phase considerations in degenerate parametric amplifier circuits, Proc. IRE 57 (1959) 1782–1783.
[47] G.L. Matthaei, Experimental verification of the phase relationships in parametric amplifiers, IEEE Trans. Micr. Theor. Tech. MTT-12 (1964) 365–367.
[48] H. Heffner, G. Wade, Gain, bandwidth and noise characteristics of a variable parameter amplifier, J. Appl. Phys. 29 (1958) 1331–1332.
[49] C.S. Aitchison, R. Davies, P.J. Gibson, A simple diode parametric amplifier design for use at S, C and X band, IEEE Trans. Micro. Theor. Tech. MTT-15 (1967) 22–31.
[50] J. Edrich, A parametric amplifier for 46 GHz, Proc. IEEE 59 (1971) 1125–1126.
[51] W.P. Connors, Maximally flat bandwidth of a nondegenerate parametric amplifier with a double tuned signal circuit and single tuned idler circuit, IEEE Trans. Micro. Theor. Tech. MTT-13 (1965) 251–252.
[52] Y. Kinoshita, M. Maeda, An 18 GHz double tuned parametric amplifier, IEEE Trans. Micro. Theor. Tech. MTT-18 (1970) 1114–1119.
[53] D.P. Howson, R.B. Smith, Parametric Amplifiers, McGraw-Hill, New York, 1970.
[54] E.S. Kuh, M. Fukada, Optimum synthesis of wide-band parametric amplifiers and converters, IRE Trans. Circ. Theor. CT-8 (1961) 410–415.
[55] G.L. Matthaei, A study of the optimum design of wide-band parametric amplifiers and up-converters, IRE Trans. Micro. Theor. Tech. MTT-9 (1961) 23–38.
[56] R.S. Engelbrecht, Nonlinear-reactance traveling-wave amplifiers for UHF, in: Tech. Dig. Solid State Circuits Conf., Philadelphia, PA, February, 1959, pp. 8–9.
[57] P.P. Lombardo, E.W. Sard, Low-frequency prototype traveling-wave reactance amplifier, Proc. IRE 47 (1959) 995–996.
[58] R.C. Honey, F.M.T. Jones, A wide-band UHF traveling-wave variable reactance amplifier, IRE Trans. Micro. Theor. Tech. MTT-8 (1960) 351–361.
[59] P.K. Tien, Parametric amplification and frequency mixing in propagating circuits, J. Appl. Phys. 29 (1958) 1347–1357.
[60] P.K. Tien, H. Suhl, A travelling-wave ferromagnetic amplifier, Proc. IRE 46 (1958) 700–706.
[61] W.H. Louisell, C.F. Quate, Parametric amplification of space charge waves, Proc. IRE 46 (1958) 707–716.
[62] R. Adler, Parametric amplification of the fast electron wave, Proc. IRE 46 (1958) 1300–1301.
[63] A. Yariv, Introduction to Optical Electronics, second ed., Holt Rinehart and Winston, New York, 1976.
[64] M.J. Feldman, P.T. Parrish, R.Y. Chiao, Parametric amplification by unbiased Josephson junctions, J. Appl. Phys. 46 (1975) 4031–4042.
[65] M. Sweeny, R. Mahler, A travelling-wave parametric amplifier utilizing Josephson junctions, IEEE Trans. Magn. MAG-21 (1985) 654–655.
[66] G. Sharma, S. Ghosh, Parametric excitation and amplification of an acoustic wave in a magnetised piezoelectric semiconductor, Phys. Stat. Sol. A 184 (2001) 443–452.
[67] J.P. Raskin, A novel parametric-effect MEMS amplifier, J. Microelectromech. Syst. 9 (2000) 528–537.
[68] B.Z. Kanevskii, V.V. Korogod, I.A. Strukov, Parametric amplifiers for radio-astronomical investigations, Radiofizika 19 (1976) 1464–1467.
[69] T.C. Hollocher, W.H. From, N.S. Bromberg, Use of a parametric amplifier in electron spin resonance spectrometer design, Phys. Med. Biol. 9 (1964) 65–72.
[70] W.M. Dougherty, K.J. Bruland, J.L. Garbini, J.A. Sidles, Detection of AC magnetic signals by parametric mode coupling in a mechanical oscillator, Meas. Sci. Technol. 7 (1996) 1733–1739.
[71] C.E. Hayes, W.A. Edelstein, J.F. Schenck, O.M. Mueller, M.J. Eash, An efficient, highly homogeneous radiofrequency coil for whole-body NMR imaging at 1,5 T, Magn. Res. 63 (1985) 622–628.

[72] J. Tropp, The theory of the bird cage resonator, J. Magn. Res. 82 (1989) 51–62.
[73] M.C. Leifer, Resonant modes of the birdcage coil, J. Magn. Res. 124 (1997) 51–60.
[74] J.T. Vaughan, G. Adriany, C.J. Snyder, J. Tian, T. Thiel, L. Bolinger, H. Liu, L. Delabarre, K. Ugurbil, Efficient high frequency body coil for high field MRI, Magn. Res. Med. 52 (2004) 851–859.
[75] R.R.A. Syms, L. Solymar, I.R. Young, Parametrically amplified magneto-inductive ring resonators, in: Proc. Metamater., Rome, 22–26 October, 2007, pp. 40–42.
[76] Philips "BB149A UHF variable capacitance diode" Product Data Sheet Rev. 03 (2004).